A Framework for Active Learning of Beam Alignment in Vehicular Millimeter Wave Communications by Onboard Sensors

Erich Zöchmann

(Christian Doppler Laboratory for Dependable Wireless Connectivity for the Society in Motion, Institute of Telecommunications, TU Wien, 1040 Vienna, Austria)

Abstract: Estimating time-selective millimeter wave wireless channels and then deriving the optimum beam alignment for directional antennas is a challenging task. To solve this problem, one can focus on tracking the strongest multipath components (MPCs). Aligning antenna beams with the tracked MPCs increases the channel coherence time by several orders of magnitude. This contribution suggests tracking the MPCs geometrically. The derived geometric tracker is based on algorithms known as Doppler bearing tracking. A recent work on geometric-polar tracking is reformulated into an efficient recursive version. If the relative position of the MPCs is known, all other sensors on board a vehicle, e.g., lidar, radar, and camera, will perform active learning based on their own observed data. By learning the relationship between sensor data and MPCs, onboard sensors can participate in channel tracking. Joint tracking of many integrated sensors will increase the reliability of MPC tracking.

Keywords: adaptive filters; autonomous vehicles; directive antennas; doppler measurement; intelligent vehicles; machine learning; millimeter wave communication

DOI: 10.12142/ZTECOM.201902002

http://kns.cnki.net/kcms/detail/34.1294.TN.20190611.1740.004.html, published online June 11, 2019

Manuscript received: 2019-04-10

1 Introduction

Millimeter wave (mmWave) frequency bands have been a candidate for vehicular communication for several decades [1]–[3]. MmWave train-to-infrastructure path loss was measured in [2], while the transmission behaviour of mmWave for communication between vehicles was examined in [1]. Recent advances in mmWave circuit technology have aroused interest in mmWave vehicular communication [3] and in joint vehicular communication and radar [4]. MmWaves offer large bandwidths and enable raw data exchange between vehicles [5]. The main problems with vehicular mmWave communication are the direct proportionality of the maximum Doppler shift and the carrier frequency as well as the beam alignment challenge in the dynamic environment. In [6] and [7], however, it has been shown theoretically that directional antennas intended for mmWaves function as spatial filters. The Doppler effect and thus the time selectivity is drastically reduced by beamforming. This is shown experimentally in [8] and [9]. There seems to be a consensus that channel tracking tackles the second challenge of the dynamic environment [10]–[21]. Channel tracking is the process of causally estimating the current or future direction of the line-of-sight (LOS) component or other strong multipath components (MPCs) based on previous measurements. The main advantage of channel tracking is the extended coherence time after successful beamforming. The channel coherence time of the beam aligned channel is several orders of magnitude longer than that for omnidirectional reception [7]. A subsequent channel estimation therefore runs on a coarser time grid.

The work in [10] adopts the idea and formalism of [21] and applies them directly to THz lens antennas. Extended Kalman filters are used in [11], [18], and [19] to track the beam directions based on channel gain measurements. In [15], domain

The work is supported by the Austrian Federal Ministry for Digital and Economic Affairs.

knowledge is used and it is argued that the road implicitly determines the direction in which a vehicle is expected. Beam training is avoided by using this geometric prior knowledge. Assuming a constant angular acceleration that is motion along circles, [20] proposes an algorithm based on the unscented Kalman filter. Probabilistic beam tracking is suggested in [16]. Moreover, in [13] and [14] the stochastic Newton method is used, and these algorithms surpass IEEE 802.11ad based approaches and compressive sensing based approaches [17]; the work in [13] and [14], shows good performance for angular velocities of up to 5°/s.

In [22], it was first proposed to utilize the Doppler information for mmWave beam tracking. Measurements in [23] clearly demonstrate that interacting objects, such as overtaking cars, produce distinguishable MPCs in the Doppler profile. The proposed algorithm herein, exploiting Doppler information, is assessed in scenarios where the angular velocity exceeds 100°/s for a short duration.

This contribution proposes to track the MPCs geometrically given quantized angular (azimuth) measurements and noisy Doppler observations. The quantized angular information is obtained by an analog or hybrid beamforming array or a dielectric lense [24]. "Geometric" refers to the (x,y) coordinates originating in the antenna array and the relative velocity $(\dot{x},\dot{y})$ to the receiver motion. We assume that the transmitter, the receiver, and the interacting objects move without acceleration. Under these assumptions, algorithms performing target-motion analysis by means of Doppler-bearing measurements [25]–[27] are directly applicable. The work in [25]–[28] proposes a formulation called "pseudolinear." Pseudolinear refers to a formulation where the nonlinearities are either hidden in a measurement (regression) matrix or are lumped within the noise term. This leads to the undesirable consequence of noise correlation of the measurements and the measurement matrix, eventually leading to biased solutions [26]. An early work [25] removes this bias by the method of instrumental variables. Due to a potential divergence of the instrumental variables approach [27], later work [26], [27] employs the method of total least squares. To apply total least squares, error covariance matrices must be known . The proposed approach is inspired by [27], but does not need knowledge about the error covariances.

In addition to the excellent angular tracking performance of the proposed algorithm, the obtained geometric information of the MPCs can be utilized to learn the MPCs from other sensors on board of automated vehicles [5]. The concept of using external information for improved channel estimation was recently reintroduced, see [29] and [30] and the reference therein. Machine learning for configuring wireless links has also been proposed in the context of WLAN and mobile communications [31]–[33]. The actual machine learning implementation is not within the scope of this contribution. This contribution focuses on a framework for active learning of beam alignment. This paper is an extended version of [34].

(1) Brief Review of Geometric Tracking or Wireless Positioning:

Ground-based radio-frequency localization has become an established technique. Based on known anchor positions, techniques such as fingerprinting, hop counts, receive signal strength, time-(difference)-of-arrival, frequency-difference-of-arrival, and angle-of-arrival are at hand [35]. Knowing the position of the communication partner is extremely valuable for the task of beam alignment [36]. In [37], a mmWave base station was equipped with a 360° camera; both positional information sources—vision and the mmWave link—were fused to enhance the precision. The situation changes however once vehicle-to-vehicle communication is considered. There, mainly GNSS positions of communication partners are exchanged by low-rate messages [38]. Future automated self-driving cars will be equipped with a plurality of sensors and will thereby perform massive sensing [5]. The smart use of all of these sensors will renders it possible to determine the position of communication partners solely by onboard sensors.

(2) Notation:

Matrices $\boldsymbol{Z}$ and vectors $\boldsymbol{z}$ are denoted by bold letters. The all zeros vector (matrix) is expressed by $\mathbf{0}$ and the identity matrix is expressed by $\boldsymbol{I}$. The Euclidean norm is symbolized by $\|\cdot\|$. A quantity defined with a start index i and stop index k is indicated via the subscript $(\cdot)_{i:k}$. Estimated quantities are marked with $(\hat{\cdot})$. The four-quadrant inverse tangent is denoted by $\arctan(\cdot,\cdot)$. The dagger $(\cdot)^{\dagger}$ is used for pseudo inverses and $(\cdot)^{T}$ is used for transposition.

2 Active Learning by Onboard Sensors

The idea behind active learning is to actively select the "optimal" training data. For some applications statistically optimal choices are computable [39]. Selective sampling [40] is a rudimentary form of active learning and especially suited for problems where the cost of labelling is high. The survey paper [41] provides a good introduction to active learning. According [41]: "The key idea behind active learning is that a machine learning algorithm can achieve greater accuracy with fewer labelled training instances if it is allowed to choose the data from which is learns."

On board of automated (self-driving) cars, there will be sensors such as global navigation satellite systems (GNSSs), automotive radars (for automatic cruise control and collision detections), lidar (for measuring distances to other objects), and 360° camera vision systems. All these sensors have in common that they track objects via target states [42]. At the simplest, this target state consists of the relative (x,y) position and the relative velocities $(\dot{x},\dot{y})$.

Due to the high-resolution of lidar, radar, and vision, self-driving cars produce several gigabytes of data per second and hence hundreds of terabytes per day [43], [44]. Processing all these data for the indented use case of driving poses already a

challenge and more and more tasks are already shifted towards fog and cloud computing units [45], [46]. To use these gigabytes of data for the tracking of MPCs, every tracked object of the onboard sensors must be labelled as "MPC" or "no MPC" (pedestrian, non-communicating car, static objects, etc.). This leads to high labelling efforts and to a huge amount of training data where most of labels will be "no MPC".

The key idea is now to exploit the geometric position of the MPC and thus to only label those targets that are in the vicinity of the MPC. The process of associating MPCs to "targets" is illustrated with black circles in **Fig. 1**. Instead of human (or any other oracle) labelling there is an active choice of the system which targets to consider for learning the beam alignment. After a successful learning phase, all sensors on board should later do the channel tracking. By using machine learning, one can eliminate or significantly reduce the beam measurements needed for the currently proposed tracking algorithm. If for all of these target states it is known whether they belong to the LOS component or to a specular reflection, the onboard sensors will track the MPCs.

In this sense this paper provides an algorithm which determines the geometric positions of the communication partners in order to label them as interesting training samples.

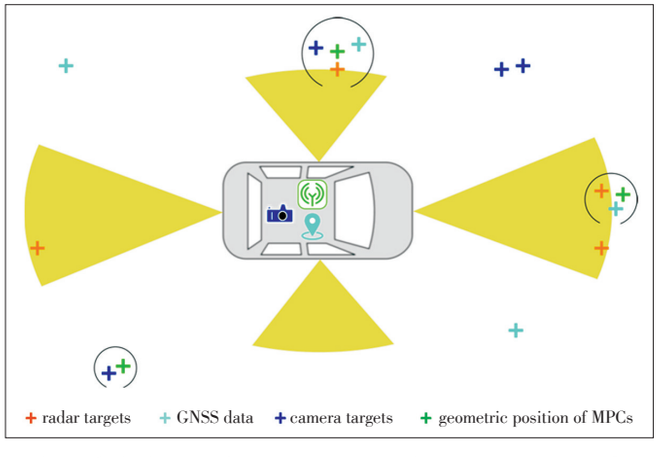

▲ Figure 1. Active learning example. The estimated state vectors of the communication link (green crosses) label the data from other sensors as a valid MPC. Therby active learning of possible beam direction from other sensors is rendered possible.

3 Measurement, Regression, and Projection Model

The regression model is based on the model proposed in [27]. The main idea of [27] is to track non-accelerating objects on linear trajectories in polar coordinates; target motion analysis in polar coordinates yields a smaller bias than in rectangular coordinates. The regression model is hence formulated in polar coordinates. This idea is illustrated in **Fig. 2**. The original tracking problem of [27] uses a running reference (blue). Thereby at each time the current state is estimated. This approach produces an increasing system of equations, anew, at any time. In contrast to [27], the proposed algorithm will use a fixed reference (red) and gather only one new equation per time step. Thereby the estimate of the initial state is refined and its accuracy is improved over time, as in [25]. Through this reformulation, the initial state-vector is estimated recursively. The state vector at current and future times is predicted by a projection.

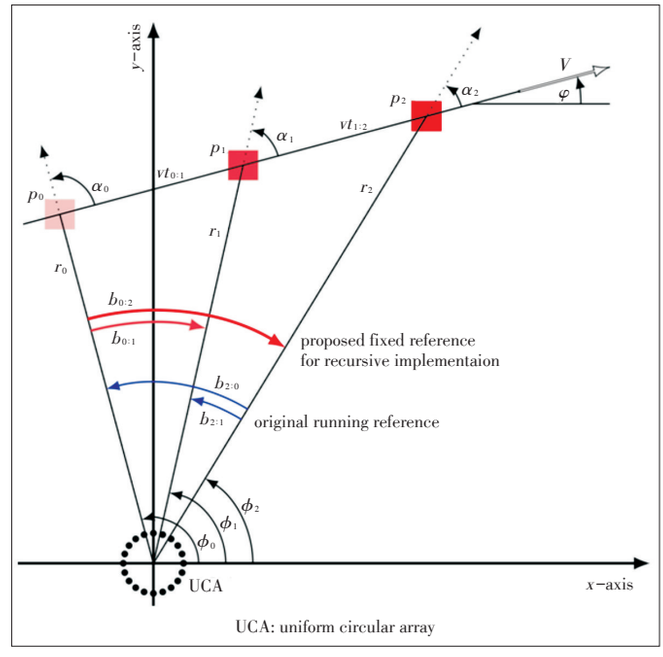

▲ Figure 2. Geometric relationship of all variables used for the algorithm. The MPC to track is marked as squqre. The employed array geometry (uniform circular array) is sketched as well.

3.1 Quantized Angular Measurements by the UCA Codebook

For target motion analysis a noisy bearing (angular) observation is assumed where the noise is usually modelled Gaussian [27]. In this study, however, quantized angular observations will occur. A 60 GHz uniform circular array (UCA) with $N=64$ elements equidistantly spaced on a radius of $r_{\mathrm{UCA}}=N/2\cdot\lambda/2\approx 8$ cm is used. The half power beam width is $\theta_{3\mathrm{dB}}\approx 2\pi/N\approx 6^{\circ}$. The UCA is inherently symmetric in its azimuthal resolution. In contrast to uniform planar arrays, the UCA beam pattern does not change with the pointing direction. To save cost, analog precoding (beamforming) with 4 bit RF phase-shifters is employed. The phase shifts are pre-computed in a codebook spaced by $\theta_{3\mathrm{dB}}/2$ which gives $2\pi/\left[(2\pi/N)/2\right]=2\cdot N=128$ codebook entries. Beampattern of the UCA are shown in **Fig. 3**.

3.2 Regression Model

The angle spanning from initial azimuth ϕ_i to the current

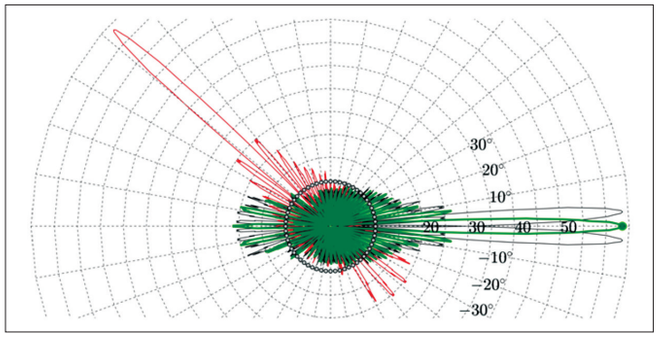

▲ Figure 3. Beampattern of the proposed uniform circular array with $N=64$ elements and 4 bit quantization of all steering vectors. The desired array pattern is marked in green; the array factor for this direction (0) is marked with a green dot; the neighbouring codebook pattern are drawn black. The uniform circular array (UCA) pattern is inherently symmetric for all directions; illustrated by the red pattern pointing in opposite direction.

azimuth ϕ_k is denoted by $b_{i:k}$. In Fig. 2, w.l.o.g. i is set to zero. The range (at time k) is denoted by r_k. The time intervals are denoted by $t_{i:k}$. The Doppler relevant angle at time k, that is α_k, is measured from the velocity vector v to the radial speed component. The basis equation is the sine law evaluated for each observation time $k>i$:

$$\frac{r_i}{\sin(\alpha_k)}=\frac{vt_{i:k}}{\sin(b_{i:k})}. \tag{1}$$

Now Equ. (1) is reformulated into a so called pseudo-linear formulation [28]:

$$\underbrace{\left[\sin(b_{i:k}),-t_{i:k}\cos(b_{i:k}),t_{i:k}\sin(b_{i:k})\right]}_{a_{B,i:k}^T}\underbrace{\begin{bmatrix}r_i\\ v\sin(\alpha_i)\\ v\cos(\alpha_i)\end{bmatrix}}_{x^i}=0, \tag{2}$$

where all nonlinearities are regressors now. For each observation-time k, one equation in the form of Equ. (2) is obtained. This is written compactly in matrix-vector notation:

$$\boldsymbol{A}_{B,i:k}\boldsymbol{x}^i=\boldsymbol{0}. \tag{3}$$

The solution to Equ. (3) is not unique. Next Doppler-shift observations ν_k are exploited. These are calculated by

$$\nu_k=\frac{v}{\lambda}\cos(\alpha_k)=\frac{v}{\lambda}\cos(\alpha_i-b_{i:k}). \tag{4}$$

Equ. (4) is re-written into the same form as Equ. (2):

$$\underbrace{\left[0,\frac{1}{\lambda}\sin(b_{i:k}),\frac{1}{\lambda}\cos(b_{i:k})\right]}_{a_{D,i:k}^T}\underbrace{\begin{bmatrix}r_i\\ v\sin(\alpha_i)\\ v\cos(\alpha_i)\end{bmatrix}}_{x^i}=v_k. \tag{5}$$

This leads again to a system of equations in form of

$$\boldsymbol{A}_{D,i:k}\boldsymbol{x}^i=\boldsymbol{\nu}_{i:k}. \tag{6}$$

One finally arrives at the augmented system of equations:

$$\begin{bmatrix}\boldsymbol{A}_{B,i:k}\\ \boldsymbol{A}_{D,i:k}\end{bmatrix}\boldsymbol{x}^i=\begin{bmatrix}\boldsymbol{0}\\ \boldsymbol{\nu}_{i:k}\end{bmatrix}. \tag{7}$$

This system of equations has a unique solution and is called "Doppler-bearing tracking" in the literature [25]–[27]. In this contribution, Equ. (7) is solved via the method of least squares (LS). Note that Equ. (7) is equivalent to

$$\begin{bmatrix}\boldsymbol{A}_{B,i:(k-1)}\\ \boldsymbol{A}_{D,i:(k-1)}\\ ----\\ \boldsymbol{a}_{B,i:k}^T\\ \boldsymbol{a}_{D,i:k}^T\end{bmatrix}\boldsymbol{x}^i=\begin{bmatrix}\boldsymbol{0}\\ \boldsymbol{\nu}_{i:(k-1)}\\ ---\\ 0\\ \nu_k\end{bmatrix}. \tag{8}$$

In Equ. (8), the previous observations are separated from the current one. This structure allows for a recursive least squares (RLS) implementation. The recursive estimate of $\boldsymbol{x}^i$ at time k will be denoted by $\hat{\boldsymbol{x}}_{i:k}^i$, in the sequel.

The angular separations $b_{i:k}$ in Equs. (1)–(8) are not known and must be estimated. The variable $b_{i:k}$ has to be replaced by $\hat{b}_{i:k}$, the estimated quantity, in the equations above. Such measurement equations are called "errors-in-variables model" in the statistics literature [47]. The estimation of $b_{i:k}$ is initially done by training sequences. For each time k, the current azimuth angle $\hat{\phi}_k$ is estimated by aid of beam sweeping, that is, a codebook scan. All possible beams are iterated and the codebook entry (azimuth direction) with largest receive power is selected. Next we obtain $\hat{b}_{i:k}=\hat{\phi}_k-\hat{\phi}_i$. Later on, onboard sensors might provide the estimate of $\hat{\phi}_k$ and codebook scans can be avoided or at least performed less frequently.

With the estimate of the initial state-vector $\hat{\boldsymbol{x}}_{i:k}^i$, we calculate the initial (x,y) position and the velocity vector $(\dot{x},\dot{y})$ based on the polar representation. The range $\hat{r}_i$ is the first element of the initial state-vector estimate, that is $\hat{\boldsymbol{x}}_{i:k}^i(1)$. The azimuth angle $\hat{\phi}_k$ is estimated through designated pilots. The velocity $\hat{v}$ is calculated through the initial state-vector estimate and the angle of the velocity vector to the x-axis φ is calculated through the initial state-vector estimate as well:

$$\begin{aligned}&\hat{v}=\sqrt{(\hat{\boldsymbol{x}}_{i:k}^i(2))^2+(\hat{\boldsymbol{x}}_{i:k}^i(3))^2},\\ &\hat{\varphi}=\hat{\alpha}_i+\hat{\phi}_i=\arctan\left\{\hat{\boldsymbol{x}}_{i:k}^i(2),\hat{\boldsymbol{x}}_{i:k}^i(3)\right\}+\hat{\phi}_i.\end{aligned} \tag{9}$$

3.3 Projection Model

A suitable projection from the initial state vector to arbitrary time points was recently derived from [48]. The assumption of a linear trajectory with non-accelerating MPCs leads to a static velocity vector. Only the range $\hat{r}_i$ and the azimuth angle $\hat{\phi}_i$ need to be projected to current (or future) time points k. The range projection $\hat{r}_k$ is calculated through [48]:

$$\hat{r}_k = \sqrt{\hat{r}_i^2 + (\hat{v}t_{i:k})^2 + 2\hat{r}_i \hat{v}t_{i:k}\cos\hat{\alpha}_i} = \sqrt{(\hat{\boldsymbol{x}}_{i:k}^i(1))^2 + t_{i:k}^2((\hat{\boldsymbol{x}}_{i:k}^i(2))^2 + (\hat{\boldsymbol{x}}_{i:k}^i(3))^2) + 2t_{i:k}\hat{\boldsymbol{x}}_{i:k}^i(1)\hat{\boldsymbol{x}}_{i:k}^i(3)}, \quad (10)$$

and the azimuth projection $\hat{\phi}_k$ is calculated through [48]

$$\hat{\phi}_k = \hat{\phi}_i + \arctan(\hat{v}t_{i:k}\sin\hat{\alpha}_i, \hat{r}_i + \hat{v}t_{i:k}\cos\hat{\alpha}_i) = \hat{\phi}_i + \arctan(t_{i:k}\hat{\boldsymbol{x}}_{i:k}^i(2), \hat{\boldsymbol{x}}_{i:k}^i(1) + t_{i:k}\hat{\boldsymbol{x}}_{i:k}^i(3)). \quad (11)$$

4 Proposed Robust Recursive Tracker

The utilized regression model falls in the following time-variant state-space model:

$$\boldsymbol{x}_{i:k}^i = \boldsymbol{x}_{i:(k-1)}^i + \boldsymbol{u}_k, \quad (12)$$

$$\underbrace{\begin{bmatrix}0\\ \boldsymbol{\nu}_k\end{bmatrix}}_{\boldsymbol{y}_k} = \underbrace{\begin{bmatrix}\boldsymbol{a}_{B,i:k}^T\\ \boldsymbol{a}_{D,i:k}^T\end{bmatrix}}_{\boldsymbol{A}_k}\boldsymbol{x}_{i:k}^i + \boldsymbol{n}_k, \quad (13)$$

where $\boldsymbol{u}_k$ is a process noise or driving disturbance with unknown distribution. The first component of the noise vector $\boldsymbol{n}_k$ stems from the quantization noise of the codebook based angle estimation. The second component is the measurement noise of the Doppler observation and is assumed to be i.i.d. zero mean Gaussian, that is, $\boldsymbol{n}_k(2) \sim N(0, 100^2)$. The high standard deviation in the Doppler noise term (100 Hz) already takes into account that current mmWave equipment suffers greatly from phase noise, see for example the measurement results in [8] and [23] or **Fig. 4** of this contribution. The assumption of zero mean Doppler noise is well justified as automated cars can use GNSS-disciplined oscillators, so that the carrier frequency offset between cars becomes very small. To increase robustness against quantization effects of the codebook and against the geometry dependent structure of $\boldsymbol{A}_k$, an $\mathcal{H}_\infty$ filter with a finite time horizon [49], [50] is applied. The objective of an $\mathcal{H}_\infty$ filter is to keep the error relation below bounded:

$$\sup_{\hat{\boldsymbol{x}}_0^i, \boldsymbol{u}, \boldsymbol{n}} \frac{\sum_{k=i}^N \|\hat{\boldsymbol{x}}_{i:k}^i - \boldsymbol{x}_{i:k}^i\|^2}{\|\hat{\boldsymbol{x}}_0^i - \boldsymbol{x}_0^i\|^2 + \sum_{k=i}^N \|\boldsymbol{u}_k\|^2 + \sum_{k=i}^N \|\boldsymbol{n}_k\|^2} < \gamma^2. \quad (14)$$

The vector $\hat{\boldsymbol{x}}_0^i$ denotes the initial guess of the state vector (in the simulations $\hat{\boldsymbol{x}}_0^i \equiv 0$, $\boldsymbol{u}_k \equiv 0$, and $\gamma = 2$). The $\mathcal{H}_\infty$ filter has a higher error floor and a higher complexity than the plain RLS solution. As a quantized codebook is used, subsequent measurements potentially provide equal azimuth angle measurements. Due to the structure of $\boldsymbol{a}_{B,i:k}$ and $\boldsymbol{a}_{D,i:k}$, the regression matrix is likely to be rank-deficient, initially. Therefore, the algorithm starts with the $\mathcal{H}_\infty$ filter and switches to the RLS filter after three different azimuth angles are measured. The recursive solution to Equ. (8) is given as

$$\hat{\boldsymbol{x}}_{i:k}^i = \hat{\boldsymbol{x}}_{i:(k-1)}^i + \boldsymbol{P}_{i:k}\boldsymbol{A}_k^T\boldsymbol{H}_{i:k}(\boldsymbol{y}_k - \boldsymbol{A}_k\hat{\boldsymbol{x}}_{i:(k-1)}^i), \quad (15)$$

where

$$\boldsymbol{H}_{i:k} = \begin{cases}\boldsymbol{I}, & for\ RLS\\ (\boldsymbol{I} + \boldsymbol{A}_k\boldsymbol{P}_{i:k}\boldsymbol{A}_k^T)^{-1}, & for\ \mathcal{H}_\infty\end{cases}. \quad (16)$$

The covariance matrix $\boldsymbol{P}_{i:k}$ fulfils the recursion (17). By aid of the Woodbury matrix identity, the inverse of the covariance matrix reveals a remarkably simple structure, see Equ. (19). Iff $\boldsymbol{P}_{i:k}^{-1}(\gamma)$ is a positive-definite matrix, the possible worst case energy (14) is bounded by γ^2 [50]. Updating $\boldsymbol{P}_{i:k}^{-1}$ and performing an inverse of a symmetric, positive-definite matrix of size 3×3 is more efficient than updating $\boldsymbol{P}_{i:k}$ directly.

$$\boldsymbol{P}_{i:k} = \begin{cases}\boldsymbol{P}_{i:(k-1)} - \boldsymbol{P}_{i:(k-1)}\boldsymbol{A}_k^T(\boldsymbol{I}_{2\times2} + \boldsymbol{A}_k\boldsymbol{P}_{i:(k-1)}\boldsymbol{A}_k^T)^{-1}\boldsymbol{A}_k\boldsymbol{P}_{i:(k-1)}, & for\ RLS\\ \boldsymbol{P}_{i:(k-1)} - \boldsymbol{P}_{i:(k-1)}\begin{bmatrix}\boldsymbol{A}_k^T & \boldsymbol{A}_k^T\end{bmatrix}\boldsymbol{R}_{e,i:k}^{-1}\begin{bmatrix}\boldsymbol{A}_k\\ \boldsymbol{A}_k\end{bmatrix}\boldsymbol{P}_{i:(k-1)}, & for\ \mathcal{H}_\infty\end{cases}, \quad (17)$$

$$\boldsymbol{R}_{e,i:k} = \begin{bmatrix}\boldsymbol{I} & \boldsymbol{0}\\ \boldsymbol{0} & -\gamma\boldsymbol{I}\end{bmatrix} + \begin{bmatrix}\boldsymbol{A}_k\\ \boldsymbol{A}_k\end{bmatrix}\boldsymbol{P}_{i:(k-1)}\begin{bmatrix}\boldsymbol{A}_k^T & \boldsymbol{A}_k^T\end{bmatrix}, \quad (18)$$

$$\boldsymbol{P}_{i:k}^{-1} = \begin{cases}\boldsymbol{P}_{i:(k-1)}^{-1} + \boldsymbol{A}_k^T\boldsymbol{A}_k, & for\ RLS\\ \boldsymbol{P}_{i:(k-1)}^{-1} + (1-\gamma^{-2})\boldsymbol{A}_k^T\boldsymbol{A}_k, & for\ \mathcal{H}_\infty\end{cases}. \quad (19)$$

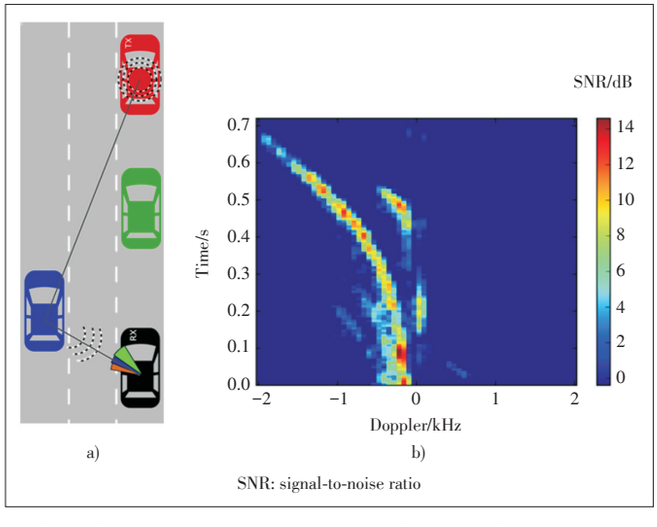

▲Figure 4. Blocked manoeuvre: a) sketch of the scenario. The green car block a direct communications between the red TX and black RX car; b) the Doppler shift estimate for this scenario obtained from a real world experiment in [9] and [23].

5 Performance Bounds-Genie Estimators

Due to quantized angular observations, the already derived Cramér-Rao bound [25] is not applicable. We will compare the obtained estimation results to two other bounds; firstly, to the "error-free regressors model." Here, the azimuth angles ϕ_k are assumed to be perfectly known, hence unquantized, and

Equ. (3) is utilized without estimates. Secondly, if the angles ϕ_k are known, Equ. (3) is not only satisfied in the least-squares sense but rather determines a solution subspace. In other words, any solution vector $\hat{\boldsymbol{x}}_{i:k}^{i}$ needs to fulfil

$$\hat{\boldsymbol{x}}_{i:k}^{i} = \left(\boldsymbol{I} - \boldsymbol{A}_{B,i:k}^{\dagger}\boldsymbol{A}_{B,i:k}\right)\boldsymbol{m},\ \boldsymbol{m} \in \mathbb{R}^3. \tag{20}$$

Now, Equ. (7) is solved by a nullspace projection:

$$\hat{\boldsymbol{x}}_{i:k}^{i,\mathrm{NS}} = \mathrm{argmin}_{\boldsymbol{m}} \left\| \boldsymbol{\nu}_{i:k} - \boldsymbol{A}_{D,i:k}\left(\boldsymbol{I} - \boldsymbol{A}_{B,i:k}^{\dagger}\boldsymbol{A}_{B,i:k}\right)\boldsymbol{m} \right\|. \tag{21}$$

As zero mean Gaussian noise is assumed for the Doppler measurements $\boldsymbol{\nu}$, the LS solution (21) is the maximum likelihood estimator of the state vector.

6 Simulations

The simulations focus on line-of-sight scenarios. Note that the proposed approach works for specular reflections as well (see next section). Clustered reflections will lead to a higher uncertainty in determining the azimuth angle. Similar to the IEEE 802.11ad standard, it is assumed that the TX is transmitting its reference signal omni-directionally. Initially, the RX is scanning all entries from the codebook and determines the direction towards the TX. We compare the performance if this procedure is repeated every 20 ms or 50 ms. After the 10th iteration, the projection (11) is used to predict the future azimuth angle. Having the projected azimuth angles at hand, the algorithm only probes the closest three codebook entries for 20 ms update rate or five codebook entries for 50 ms update rate. This gives a speed up of a factor $128/3 \approx 43$ or $128/5 \approx 26$ as compared to a full codebook scan.

The first scenario, entitled "half-overtaking", starts when the overtaking, red, TX car is at the same height as the slower, black, RX car. The overtaking car has 20 m/s excess speed and is observed for 3 s. In the second scenario, entitled "full-overtaking", the TX starts behind the RX and overtakes with an excess speed of 10 m/s. The manoeuvre is now observed for 6 s. The lateral distance was chosen such that the resulting maximum angular velocity $\omega_{\max} = v/r_{\min} = (20\ \mathrm{m/s})/(8\ \mathrm{m}) = (10\ \mathrm{m/s})/(4\ \mathrm{m}) = 2.5\ \mathrm{rad/s} \approx 140^{\circ}/\mathrm{s}$ is equal in both scenarios. The presented Monte Carlo mean is calculated from 10 000 runs. To obtain different channel realizations, the lateral distance is varied uniformly in $\Delta r_{\min} \sim U(-1\ \mathrm{m}, 1\ \mathrm{m})$ around the mean lateral distances, and the angle between both cars is varied uniformly in $\varphi \sim U\left(-2^{\circ}, 2^{\circ}\right)$. These variations are drawn within the sketch of the manoeuvre as black arrows in **Fig. 5a**. The normalized mean squared error of the prior work [27], the proposed sequential implementation from Section 4, and both error bounds from Section 5 are plotted in **Figs. 5c** (20 ms update rate) and **5e** (50 ms update rate). **Figs. 5b** and **5d** show the respective scatter plots of the estimated (x, y) position of the proposed sequential estimator for the first Monte Carlo run.

Half overtaking (with update rate of 20 ms) turns out to be not so burdensome than full-overtaking. That is because right from the beginning, the TX car is seen at different azimuth angles and close to the initial solution of (0,0) and the algorithm convergences fast. The regression model of [27] suffers from a strong bias due to the error correlation of the current observation and the regression matrix. The sequential algorithm outperforms the prior non-sequential modelling approach. The "errors-in-variables" approach comes very close to the error-free regression matrix. Furthermore, there is only a small loss to the nullspace projection. Keep in mind that the "error-free regressors" and the nullspace projection approach make use of exact (yet unknown), unquantized azimuth angles! The full overtaking manoeuvre is characterized by a difficult geometry. At the beginning the TX car is always seen at the same codebook index and the algorithm struggles to converge. In this region the $\mathcal{H}_{\infty}$ algorithm is used to prevent divergence. After approximately 0.5 s, three different azimuth angles have been measured and the algorithm hands over to RLS. Even with an estimate of the initial state and the covariance matrix, the RLS algorithm needs a considerable time to converge afterwards. The situation is aggravated by the fact that the toughest part (TX car closest to RX car $\rightarrow \omega_{\max}$) comes before convergence sets in. Nevertheless, an acceptable tracking result can be achieved here as well.

For an update rate of 50 ms the peformance loss at "full-overtaking" is minor. In contrast, the previously simpler case of "half-overtaking" has now a larger performance loss. Due to the slower update rate, after only a few measurements, the overtaking car is already at steeper angles where the Doppler shift does not change so much and convergence is harder to achieve.

7 The LOS Blocked Scenario

Until now, all cases considered LOS. The proposed tracker, however, is also applicable to scenarios with specular reflections. Fig. 4 shows a blockage scenario. The direct LOS between TX (the red car) and RX (the black car) is blocked by the green car. If another car overtakes this platoon, it can act as reflector and can be tracked by its Doppler shift. The feasibility of this approach has been verified experimentally in [9] and [23]. The Doppler shifts of overtaking vehicles produce very distinct Doppler traces. Such an exemplary trace is illustrated on the right-hand side of Fig. 4. The only adaptation for the algorithm is a factor 2 occuring in the Doppler shift equations.

8 Conclusions

Geometric tracking of specular multipath components in vehicular millimeter wave channels is possible with low complexity algorithms. The proposed algorithm achieves good tracking even under very dynamic scenarios. This considerably relaxes

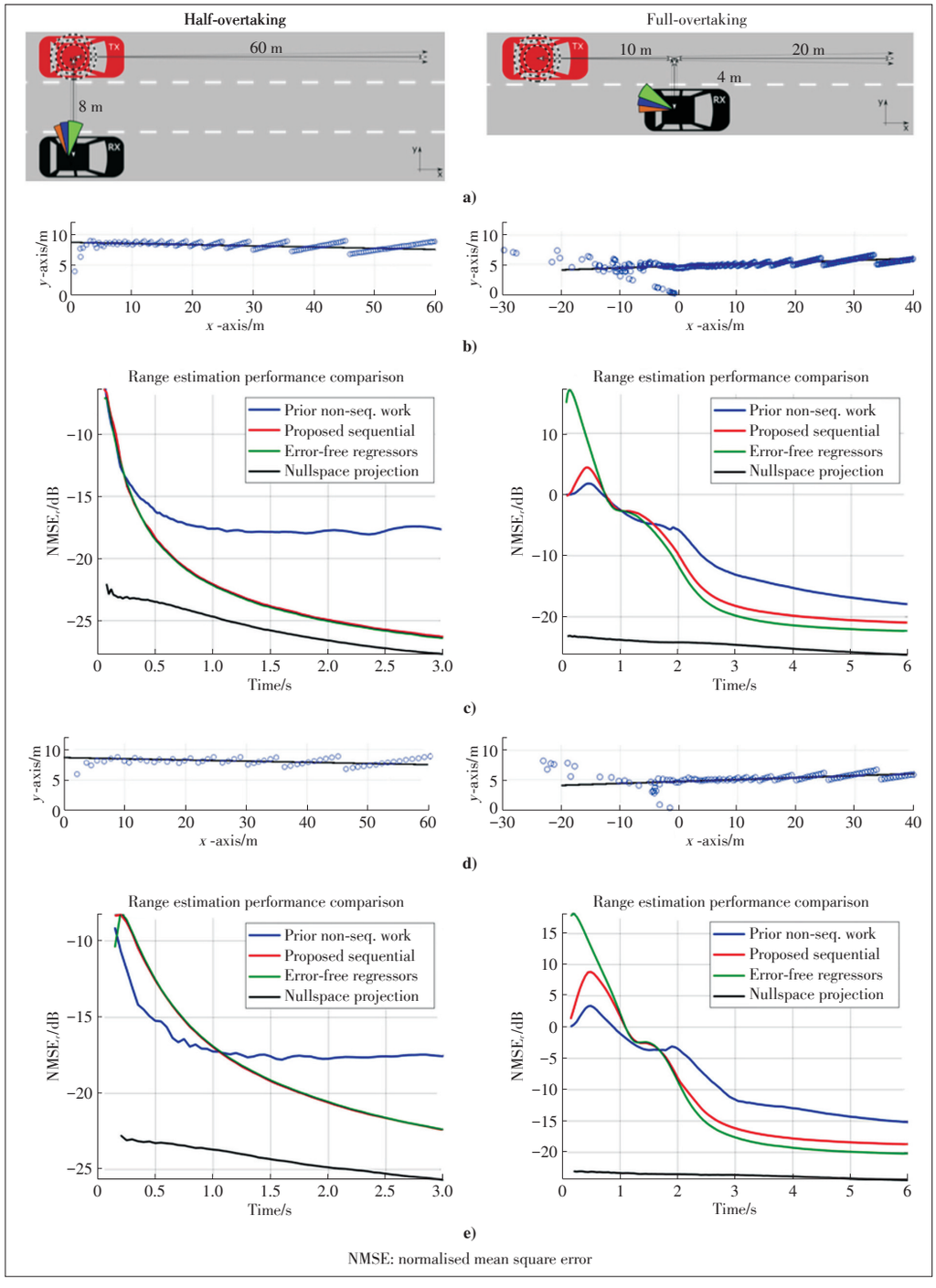

◀**Figure 5. a) Manoeuvre sketch of the scenarios; b) exemplary relative position estimates (x,y) of the proposed estimator with 20 ms update rate; c) range normalized mean squared error comparisons with 20 ms update rate; d) (x,y) estimates with 50 ms update rate; e) NMSE with 50 ms update rate**

the time required for beam training. In addition, the proposed algorithm outputs a state vector that reflects the relative position and velocity of the multipath components. With this knowledge, it is possible to label the targets for onboard sensors as multipath components. This enables active learning for onboard sensors.

References

[1] AKIHITO K, KATSUYOSHI S, FUJISE M, et al. Propagation Characteristics of 60-GHz Millimeter Waves for ITS Inter-Vehicle Communications [J]. IEICE Transactions on Communications, 2001, 84(9): 2530–2539
[2] MEINEL H, PLATTNER A. Millimeter-Wave Propagation along Railway Lines [J]. IEE Proceedings F (Communications, Radar and Signal Processing), 1983, 130(7): 688. DOI: 10.1049/ip-f-1.1983.0102
[3] VA V, SHIMIZU T, BANSAL G, et al. Millimeter Wave Vehicular Communications: A Survey [J]. Foundations and Trends in Networking, 2016, 10(1): 1–113. DOI:10.1561/1300000054
[4] KUMARI P, CHOI J, GONZALEZ-PRELCIC N, et al. IEEE 802.11ad-Based Radar: An Approach to Joint Vehicular Communication-Radar System [J]. IEEE Transactions on Vehicular Technology, 2018, 67(4): 3012–3027. DOI: 10.1109/

tvt.2017.2774762
[5] CHOI J, VA V, GONZALEZ-PRELCIC N, et al. Millimeter-Wave Vehicular Communication to Support Massive Automotive Sensing [J]. IEEE Communications Magazine, 2016, 54(12): 160–167. DOI: 10.1109/mcom.2016.1600071cm
[6] LORCA J, HUNUKUMBURE M, WANG Y. On Overcoming the Impact of Doppler Spectrum in Millimeter-Wave V2I Communications [C]//2017 IEEE Globecom Workshops. Singapore, Singapore, 2017: 1– 6. DOI: 10.1109/GLOCOMW.2017.8269039
[7] VA V, CHOI J, HEATH R W. The Impact of Beamwidth on Temporal Channel Variation in Vehicular Channels and Its Implications [J]. IEEE Transactions on Vehicular Technology, 2017, 66(6): 5014–5029. DOI: 10.1109/tvt.2016.2622164
[8] ZÖCHMANN E, HOFER M, LERCH M, et al. Statistical Evaluation of Delay and Doppler Spread in 60 GHz Vehicle-To-Vehicle Channels during Overtaking [C]//2018 IEEE-APS Topical Conference on Antennas and Propagation in Wireless Communications (APWC), Cartagena des Indias, Colombia, 2018: 1– 4. DOI: 10.1109/APWC.2018.8503750
[9] ZOCHMANN E, HOFER M, LERCH M, et al. Position-Specific Statistics of 60 GHz Vehicular Channels during Overtaking [J]. IEEE Access, 2019, 7: 14216–14232. DOI:10.1109/access.2019.2893136
[10] GAO X Y, DAI L L, ZHANG Y, et al. Fast Channel Tracking for Terahertz Beamspace Massive MIMO Systems [J]. IEEE Transactions on Vehicular Technology, 2017, 66(7): 5689–5696. DOI: 10.1109/tvt.2016.2614994
[11] JAYAPRAKASAM S, MA X X, CHOI J W, et al. Robust Beam-Tracking for mmWave Mobile Communications [J]. IEEE Communications Letters, 2017, 21 (12): 2654–2657. DOI: 10.1109/lcomm.2017.2748938
[12] LI J H, SUN Y, XIAO L M, et al. Analog Beam Tracking in Linear Antenna Arrays: Convergence, Optimality, and Performance [C]//51st Asilomar Conference on Signals, Systems, and Computers. Pacific Grove, USA, 2017: 1193– 1198. DOI: 10.1109/ACSSC.2017.8335540
[13] LI J H, SUN Y, XIAO L M, et al. Super Fast Beam Tracking in Phased Antenna Arrays: Theory and Performance [EB/OL]. (2017-10-22). https://arxiv.org/abs/1710.07873
[14] LI J H, SUN Y, XIAO L M, et al. How to Mobilize Mmwave: A Joint Beam and Channel Tracking Approach [C]//IEEE International Conference on Acoustics, Speech and Signal Processing (ICASSP). Calgary, Canada, 2018: 3624–3628. DOI:10.1109/ICASSP.2018.8461760
[15] LOCH A, ASADI A, SIM G H, et al. Mm-Wave on Wheels: Practical 60 GHz Vehicular Communication without Beam Training [C]//9th International Conference on Communication Systems and Networks (COMSNETS). Bangalore, India, 2017: 1–8. DOI:10.1109/COMSNETS.2017.7945351
[16] PALACIOS J, DE DONNO D, WIDMER J. Tracking mm-Wave Channel Dynamics: Fast Beam Training Strategies under Mobility [C]//IEEE Conference on Computer Communications (INFOCOM). Atlanta, USA, 2017: 1– 9. DOI: 10.1109/INFOCOM.2017.8056991
[17] RODRÍGUEZ-FERNÁNDEZ J, GONZÁIEZ-PRELCIC N, HEATH R W. Frequency-Domain Wideband Channel Estimation and Tracking for Hybrid MIMO Systems [C]//51st Asilomar Conference on Signals, Systems, and Computers. Pacific Grove, USA, 2017: 1829–1833. DOI: 10.1109/ACSSC.2017.8335678
[18] VA V, VIKALO H, HEATH R W. Beam Tracking for Mobile Millimeter Wave Communication Systems [C]//IEEE Global Conference on Signal and Information Processing (GlobalSIP). Washington, DC, USA, 2016: 743– 747. DOI: 10.1109/GlobalSIP.2016.7905941
[19] ZHANG C, GUO D N, FAN P Y. Tracking Angles of Departure and Arrival in a Mobile Millimeter Wave Channel [C]//IEEE International Conference on Communications (ICC). Kuala Lumpur, Malaysia, 2016: 1– 6. DOI:10.1109/ICC.2016.7510902
[20] ZHAO J W, GAO F F, JIA W M, et al. Angle Domain Hybrid Precoding and Channel Tracking for Millimeter Wave Massive MIMO Systems [J]. IEEE Transactions on Wireless Communications, 2017, 16(10): 6868– 6880. DOI: 10.1109/twc.2017.2732405
[21] ZHOU Y F, YIP P C, LEUNG H. Tracking the Direction-Of-Arrival of Multiple Moving Targets by Passive Arrays: Algorithm [J]. IEEE Transactions on Signal Processing, 1999, 47(10): 2655–2666. DOI: 10.1109/78.790648
[22] ZÖCHMANN E, CABAN S, LERCH M, et al. Resolving the Angular Profile of 60 GHz Wireless Channels by Delay-Doppler Measurements [C]//IEEE Sensor Array and Multichannel Signal Processing Workshop (SAM). Rio de Janerio, Brazil, 2016: 1–5. DOI:10.1109/SAM.2016.7569652
[23] ZÖCHMANN E, MECKLENBRÄUKER C F, LERCH M, et al. Measured Delay and Doppler Profiles of Overtaking Vehicles at 60 GHz [C]//12th European Conference on Antennas and Propagation (EuCAP). London, UK: 1–5, 2018. DOI: 10.1049/cp.2018.0470
[24] ZENG Y, ZHANG R. Millimeter Wave MIMO with Lens Antenna Array: A New Path Division Multiplexing Paradigm [J]. IEEE Transactions on Communications, 2016, 64(4): 1557–1571. DOI: 10.1109/tcomm.2016.2533490
[25] CHAN Y T, RUDNICKI S W. Bearings-Only and Doppler-Bearing Tracking Using Instrumental Variables [J]. IEEE Transactions on Aerospace and Electronic Systems, 1992, 28(4): 1076–1083. DOI: 10.1109/7.165369
[26] HO K C, CHAN Y T. An Asymptotically Unbiased Estimator for Bearings-Only and Doppler-Bearing Target Motion Analysis [J]. IEEE Transactions on Signal Processing, 2006, 54(3): 809–822. DOI: 10.1109/tsp.2005.861776
[27] HO K C, CHAN Y T. Geometric-Polar Tracking from Bearings-Only and Doppler-Bearing Measurements [J]. IEEE Transactions on Signal Processing, 2008, 56(11): 5540–5554. DOI: 10.1109/tsp.2008.928701
[28] RAO S K. Pseudo-Linear Estimator for Bearings-Only Passive Target Tracking [J]. IEE Proceedings—Radar, Sonar and Navigation, 2001, 148(1): 16. DOI: 10.1049/ip-rsn:20010144
[29] ALIEIEV R, HEHN T, KWOCZEK A, et al. Predictive Communication and Its Application to Vehicular Environments: Doppler-Shift Compensation [J]. IEEE Transactions on Vehicular Technology, 2018, 67(8): 7380–7393. DOI: 10.1109/tvt.2018.2835662
[30] GONZALEZ-PRELCIC N, ALI A, VA V, et al. Millimeter-Wave Communication with Out-Of-Band Information [J]. IEEE Communications Magazine, 2017, 55(12): 140–146. DOI: 10.1109/mcom.2017.1700207
[31] DANIELS R C, CARAMANIS C M, HEATH R W. Adaptation in Convolutionally Coded MIMO-OFDM Wireless Systems through Supervised Learning and SNR Ordering [J]. IEEE Transactions on Vehicular Technology, 2010, 59(1): 114–126. DOI: 10.1109/tvt.2009.2029693
[32] DJOUAMA A, ZÖCHMANN E, PRATSCHNER S, et al. Predicting CSI for Link Adaptation Employing Support Vector Regression for Channel Extrapolation [C]//20th International ITG Workshop on Smart Antennas (WSA 2016). Munich, Germany, 2016: 1–7
[33] VA V, CHOI J, SHIMIZU T, et al. Inverse Multipath Fingerprinting for Millimeter Wave V2I Beam Alignment [J]. IEEE Transactions on Vehicular Technology, 2018, 67(5): 4042–4058. DOI: 10.1109/tvt.2017.2787627
[34] ZÖCHMANN E, VA V, RUPP M, et al. Geometric Tracking of Vehicular mmWave Channels to Enable Machine Learning of Onboard Sensors [C]//2018 IEEE Globecom Workshops. Abu Dhabi, United Arab Emirates, 2018: 1–6. DOI: 10.1109/GLOCOMW.2018.8644440
[35] TAHAT A, KADDOUM G, YOUSEFI S, et al. A Look at the Recent Wireless Positioning Techniques with a Focus on Algorithms for Moving Receivers [J]. IEEE Access, 2016, 4: 6652–6680. DOI: 10.1109/access.2016.2606486
[36] SHAHMANSOORI A, GARCIA G E, DESTINO G, et al. Position and Orientation Estimation through Millimeter-Wave MIMO in 5G Systems [J]. IEEE Transactions on Wireless Communications, 2018, 17(3): 1822– 1835. DOI: 10.1109/twc.2017.2785788
[37] TRULLENQUE ORTIZ M, et al. Vehicle Tracking Through Vision-Millimeter Wave Doppler Shift Fusion [Z]. to be published at IEEE-APS APWC, 2019.
[38] HOANG M G, DENIS B, HÄRRI J, et al. (2015). Distributed Link Selection and Data Fusion for Cooperative Positioning in GPS-Aided IEEE 802.11p VANETs [C]//12th Workshop on Positioning, Navigation and Communication. Dresden, Germany, 2015
[39] COHN D, GHAHRAMANI Z, JORDAN M J. Active Learning with Statistical Models [J]. Journal of Artificial Intelligence Research, 1996, 4: 129–145. DOI: 10.1613/jair.295
[40] COHN D, ATLAS L, LADNER R. Improving Generalization with Active Learning [J]. Machine Learning, 1994, 15(2): 201–221. DOI: 10.1007/bf00993277
[41] SETTLES B. Active Learning Literature Survey [R/OL]. (2010-01-26). http://burrsettles.com/pub/settles.activelearning.pdf
[42] ROCKL M, STRANG T, KRANZ M. V2V Communications in Automotive Multi-Sensor Multi-Target Tracking [C]//IEEE 68th Vehicular Technology Conference. Calgary, Canada, 2008: 1–5. DOI: 10.1109/VETECF.2008.440
[43] GRZYWACZEWSKI A. NVIDIA Corporation: Training AI for Self-Driving Vehicles: the Challenge of Scale [R/OL]. (2017). https://devblogs.nvidia.com/parallelforall/training-self-driving-vehicles-challenge-scale
[44] LIU S S, TANG J, ZHANG Z, et al. Computer Architectures for Autonomous Driving [J]. Computer, 2017, 50(8): 18–25. DOI: 10.1109/mc.2017.3001256
[45] HUANG C, LU R X, CHOO K-K R. Vehicular Fog Computing: Architecture, Use Case, and Security and Forensic Challenges [J]. IEEE Communications Magazine, 2017, 55(11): 105–111. DOI: 10.1109/mcom.2017.1700322
[46] KONG L H, KHAN M K, WU F, et al. Millimeter-Wave Wireless Communications for IoT-Cloud Supported Autonomous Vehicles: Overview, Design, and Challenges [J]. IEEE Communications Magazine, 2017, 55(1): 62–68. DOI:

➡To P. 58

[7] IEC. Digital Data Communications for Measurement and Control—Fieldbus for Use in Industrial Control Systems: IEC 61158 [S]. 2003
[8] TONG W M, MU M, LIN J-B. Fieldbus Standard [J]. Low Voltage Apparatus, 2003(2): pp. 32-36. DOI: 10.3969/j.issn.1001-5531.2003.02.009
[9] IEC/TC Delegation of China. IEC SC65C MT9, WG11 Fieldbus and Real-time Ethernet Working Group Meeting (USA) Minutes [J]. Instrument Standardization and Metrology, 2006(1). DOI: 10.3969/j.issn.1672-5611.2006.01.003
[10] WINKEL L. Real-Time Ethernet in IEC 61784-2 and IEC 61158 Series [C]// 4th IEEE International Conference on Industrial Informatics, Singapore, Singapore, 2006: 246-250. DOI:10.1109/INDIN.2006.275788
[11] IEC. Industrial Communication Networks—Fieldbus Specifications—Part 1: Overview and Guidance for the IEC 61158 and IEC 61784 Series: IEC 61158 [S]. 2014
[12] MIAO X Q. The Latest Development in Real-Time Ethernet Technology [J]. Electrical Age, 2005(6): pp. 64- 68. DOI: 10.3969/j.issn.1000 -453X.2005.06.018
[13] IEC. Low Voltage Switchgear and Controlgear—Controller Device Interfaces (CDIs): IEC62026 [S]. 2008
[14] ISO. Road Vehicles—Controller Area Network (CAN): ISO 11898 [S]. 2015
[15] ISO. Road Vehicles—Low-Speed Serial Data Communication—Part 3:Vehicle Area Network: ISO 11519 [S]. 1995
[16] GUO Q Y, HUANG S Z, XUE J. The Applications of Fieldbus and Industrial Ethernet [M]. Beijing, China: Science Press, 2016.
[17] DEMARTINI C, VALENZANO A. The EN50170 Standard for a European Fieldbus [J]. Computer Standards & Interfaces, 1998, 19(5/6): 257-273. DOI: 10.1016/s0920-5489(98)00027-0
[18] TIAN M, GAO A B. New Development of "LonWorks" Fieldbus Technology [J]. Journal of Harbin University of Science and Technology, 2010, 15(1): 33-39. DOI: 10.3969/j.issn.1007-2683.2010.01.008
[19] NIE X B, WANG L D, SHEN P, et al. Real-Time Performance Analysis and Research of ARCNET Network System [J]. Journal of the China Railway Society, 2011, 33(1): pp. 58-62. DOI: 10.3969/j.issn.1001-8360.2011.01.010
[20] GAO Z B, XU G J, WANG B. Implementation of Signal Acquisition System Based on Siemens PLC and Dupline Bus [J]. Nonferrous Metals: Mineral Processing, 2017, 206: 204-206. DOI: 10.3969/j.issn.1671-9492.2017.z1.045

Biographies

CHEN Jinghe (16121422@bjtu.edu.cn) received her Bachelor's degree in electrical engineering from Jinan University, GuangDong in 2016. Now she is a master in electrical engineering of Beijing Jiaotong University, China, and she engages in research of fieldbus and industrial Ethernet.

ZHANG Hesheng received his B.S.E.E. and M.S. degrees in electrical engineering from Northern Jiaotong University of China in 1992 and 1995, respectively. He received his Ph.D. degree in automation science and technology from Tsinghua University, China in 2006. He is now a professor in School of Electrical Engineering, Beijing Jiaotong University, China. His research interests include fieldbus, sensor network, network communication performance, and intelligent control. He is a senior member of the CES and CCF. He has published more than 60 papers in the journals and conferences as the first or second author, and has applied for nine national invention patents as the first inventor.

←From P. 09

10.1109/mcom.2017.1600422cm
[47] CARROLL R J, RUPPERT D, CRAINICEANU C M, et al. Measurement Error in Nonlinear Models: A Modern Perspective [M]. London, UK: Chapman and Hall/CRC, 2006
[48] BATTISTELLI G, CHISCI L, FANTACCI C, et al. Networked Target Tracking with Doppler Sensors [J]. IEEE Transactions on Aerospace and Electronic Systems, 2015, 51(4): 3294-3306. DOI: 10.1109/taes.2015.140340
[49] HASSIBI B, SAYED A H, KAILATH T. Indefinite-Quadratic Estimation and Control: A Unified Approach to H2 and H-infinity Theories [M]. Philadelphia, USA: SIAM, 1999: vol 16
[50] KAILATH T, SAYED A H, HASSIBI B. Linear Estimation [M]. Upper Saddle River, USA: Prentice Hall, 2000

Biography

Erich Zöchmann (ezoechma@gmail.com) received all his degrees (B.Sc., Dipl.-Ing, Dr.techn) in electrical engineering from TU Wien, Austria. From 2013 to 2015, he was a project assistant at the Institute of Telecommunications where he co-developed the Vienna LTE-A uplink link level simulator and conducted research on physical layer signal processing for 4G mobile communication systems. From 2015 to 2018 he was involved in experimental characterization and modelling of millimeter wave propagation. From November 2017 until February 2018, he was a visiting scholar at the University of Texas at Austin, USA. Besides wireless propagation, his research interests include physical layer signal processing, array signal processing, compressed sensing, and convex optimization.